SAE TECHNICAL
PAPER SERIES

2002-01-0059

Optimization of Exhaust Systems

Meda Lakshmikantha and Mathias Kec
Eberspaecher North America, Inc.

Reprinted From: Emissions Modeling and General Emissions (SP–1676)

The Engineering Society For Advancing Mobility Land Sea Air and Space®
INTERNATIONAL

SAE 2002 World Congress
Detroit, Michigan
March 4-7, 2002

400 Commonwealth Drive, Warrendale, PA 15096-0001 U.S.A. Tel: (724) 776-4841 Fax: (724) 776-5760

ISSN 0148-7191

Printed in USA

2002-01-0059

Optimization of Exhaust Systems

Meda Lakshmikantha and Mathias Keck
Eberspaecher North America, Inc.

ABSTRACT:

Some design optimization studies of automotive exhaust systems are carried out using numerical simulation. The numerical simulation involves computational fluid dynamics (CFD) for fluid flow and temperature distribution and finite element analysis (FEA) for subsequent structural analysis. The emphasis is given to optimization related to exhaust system design parameters such as shape and profile of manifold, catalyst inlet tube, inlet cone, exit cone, and exit tube under a given exhaust gas conditions. Several examples of optimization involving study of design parameters on the index of flow uniformity and backpressure are illustrated. Some studies in the past have shown that angular inflow in to catalyst substrate would give high flow uniformity index and flow out let profiles may not significantly affect the uniformity flow index near the inlet of catalyst. The present study shows that this is not always the case and some examples are illustrated to highlight these aspects.

The second part of this study involves finite element calculation of stresses and strains. Due to high temperatures involved in the exhaust system both material and geometric non-linearity are considered in structural analysis. Specifically, the study involves the calculation of material response behavior under several thermal cycles, each cycle involving a heating and a cooling stages, and finally comparative study of suitability of cast steel and fabricated steel for exhaust manifolds are discussed.

INTRODUCTION:

Several factors have contributed to increase in activities related to optimization of exhaust systems. These are: market forces to decrease the cost, requirements of high service life & improved performance. The emissions are high in the first few seconds after the cold start when the under floor catalysts are cold and inactive. This necessitated the use of close-coupled converter (cc-converter). These converters are located close to the engine to warm up the catalyst quickly. But the available space is limited. The space-constraints affect the system designs. Hence it is important to understand the effect of system designs on the flow distribution near the inlet region of the converter.

Past studies [1,4] have shown that uniform distribution of exhaust gases near the inlet cross section of the catalyst resulted in improved conversion. Further, the deposition rate depends to the local gas velocity and better flow distribution results in more uniform deposition near the inlet of the catalyst. Thus catalytically active cells near the central region of the monolith are less covered. This helps in improving the

service life of the catalyst. The uniform velocity distribution also enables shallow temperature gradients in the monolith and this results in increased life of the monolith.

The flow distribution near the inlet of the monolith of cc-converter depends on the shape & profile of the manifold upstream of the converter, geometry and size of the tube connection to the inlet cone of the converter, viscous and inertial resistance of the monolith, and also on the geometry of the tube down stream of the converter. In the past several studies [1-3] have been made on behavior of exhaust gases in the underflow converter and close-coupled converter. In addition to these, this paper describes in detail about the effect of geometry of different components such as manifold, inlet tube, inlet cone, and outlet cone & tube on the flow distribution.

Once the exhaust system is optimized for flow, the next logical step is to make sure that the manifold design is structurally sound [5-7] to with stand the exhaust gas pulsations and cooling stages. The exhaust manifolds are placed close to the engine in close-coupled converter designs. This results in subjecting the manifolds to thermal fluctuations from gases of the engine cylinders. The manifolds have to withstand the heating from room temperature to maximum exhaust gas temperatures of up to 950 C. Further manifolds are subjected to thermal pulsations from each cylinder. After several thousand heating pulsations, when the engine is stopped, the manifold is brought down to room temperature. This may result in residual stresses in the manifold. Hence study of behavior of manifold under thermal pulsations due to exhaust from several cylinders and structural response of manifold under several cycles are needed. Further the effect of several cycles involving heating & cooling on the behavior of manifold is carried out. In addition to this, the manifold materials cast stainless steel and hydroformed/fabricated stainless steel is studied to illustrate the difference between them especially when high temperatures are involved.

FLOW CALCULATIONS:

Figure 1 shows the sketch of a close-coupled exhaust manifold system considered here for the study. The system involved manifold, inlet tube, inlet cone, catalyst, and exit cone and exit tube. The monolith is made of ceramic material and has a cell density of 600 cells/inch 2 (600 cpsi).

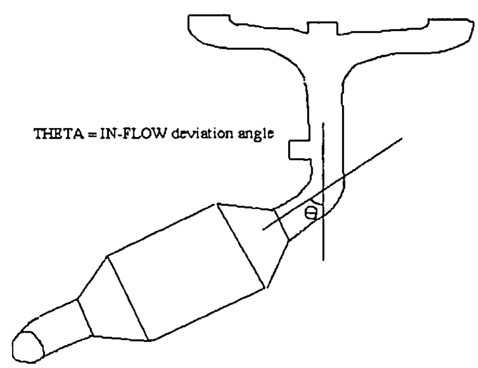

Figure 1. The sketch of exhaust system used in this flow simulation study. The angle between the exit of manifold and converter inlet tube is defined as in-flow deviation angle.

The walls of these cells are wash-coated and are not penetrated by exhaust gases. The monolith is modeled as a porous medium with only axial laminar flow and no radial mass transfer. The porous medium is represented using the pressure loss per unit length. No reaction is considered in the analysis. The exhaust system is modeled from the inlet of manifold to the outlet of catalyst including exit tube. Flow is considered turbulent and standard k-e model is used in the analysis. As indicated earlier, flow uniformity in front of the monolith is an important parameter in the analysis of exhaust systems. Flow uniformity at a cross section is represented by an index called, flow uniformity index. This is defined as:

Uniformity index,

$$\gamma = 1 - \sum \left| \varpi_i - \varpi \right| a_i \; / \; 2\varpi A$$

a_i: cross sectional area of the cell i

A: cross sectional area of the monolith

ϖ: average velocity

ϖ_i: average velocity on the cell i

The value of uniformity index in exhaust systems is usually between 0.65 and 0.98. More the flow uniformity, higher the uniformity indexes.

INFLUENCE OF EXHAUST FROM DIFFERENT CYLINDERS:

The boundary conditions such as mass flow rate, temperature and exit pressure are obtained from one-dimensional engine wave calculations.

The exhaust from cylinder 2, 4 and 6 at 6500 RPM gives uniformity index values of 0.845, 0.927 and 0.946 respectively at a section about 30 mm inside the monolith from the front face of the monolith. Figures 2 and 3 shows the velocity path lines for exhaust from cylinders 6 and 2. It can be seen that, although the manifold head corresponding cylinder 2 looks similar to cylinder 6, it is clear that the flow from cylinder 2 creates flow separation in front of the monolith and this in turn makes the flow more non-uniform near the entrance region of the monolith.

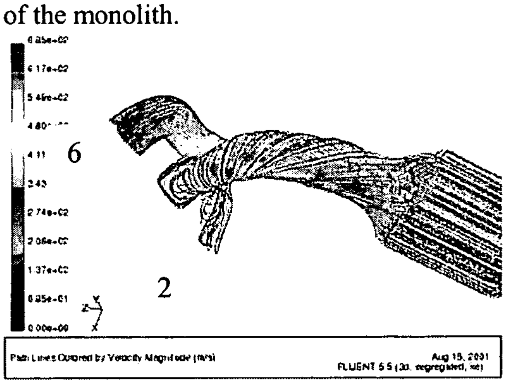

Figure 2. Velocity path lines due to exhaust from cylinder 6.

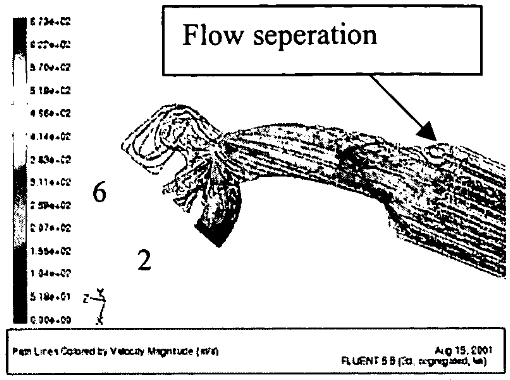

Figure 3. Velocity path lines due to exhaust from cylinder 2.

Table 1 shows the values of uniformity index and total pressure drop from the inlet to out let. It can be seen from the table 1, that the exhaust from cylinder 2 produces the maximum total pressure drop. Also flow from cylinder 4 produces the lowest total pressure drop since the exhaust from cylinder 4 goes through relatively less number of joints where the flow change its angle.

	Cyl. 2	Cyl. 4	Cyl. 6
Gamma	0.845	0.927	0.946
Total pressure drop (mbars)	529	161	508

Table 1. Uniformity index, Gamma and total pressure drop for exhausts from cylinders 2, 4 & 6.

INFLUENCE OF EXIT TUBE:

The same manifold with the exit tube reversed can be used for exhaust from cylinders 1, 3 and 5. In this case similar analysis is performed with the exit tube reversed. The results for this case are shown in Table 2.

	Cyl. 1 (2)	Cyl. 3 (4)	Cyl. 5 (6)
Gamma	0.886	0.943	0.945
Total pressure drop (mbars)	516	163	499

Table 2. Uniformity index, Gamma and total pressure drop for exhausts from cylinders 1, 3 & 5.

It can be seen from Table 2 that the gamma values improve from 0.845 to 0.88 corresponding to cylinder 2 and from 0.927 to 0.943 for cylinder 4. This shows that exit tube behind the manifold can affect the flow characteristics in front of monolith.

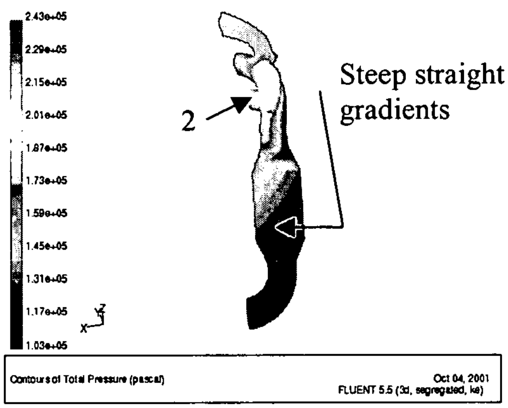

Figure 4. Total pressure contours for exhaust flow from cylinder 2 (1).

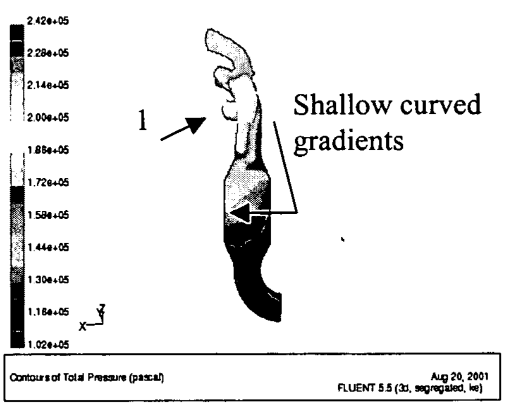

Figure 5. Total pressure contours for exhaust flow from cylinder 1.

Figures 4 and 5 show total pressure contours for exhaust flow from cylinders 2 and 1. In Figure 4, the total pressure contours have steep straight contours on the monolith walls. In contrast, from Figure 5, in the exit tube reversed case, the total pressure contours have relatively shallow curved pressure gradients suggesting a improved flow uniformity inside the monolith. Since gamma is directly related to Reynolds number, lower velocity near the entrance of monolith improves the gamma value.

INFLUENCE OF IN-FLOW DEVIATION ANGLE:

It can be seen from Figure 1 that flow deviates and changes the flow angle at a joint just upstream of the converter. Few more design analyses are performed to obtain an optimum flow deviation angle corresponding to maximum uniformity index by changing the flow angles at the joint. The position of the bend with respect to cone is kept constant for all flow deviation angles.

Figure 6 shows the variation of gamma values as the flow deviation angle is changed. It can be seen from this figure that at zero flow deviation angle, uniformity index have the lowest value for exhaust from cylinders 2, 4 and 6. Further, gamma values

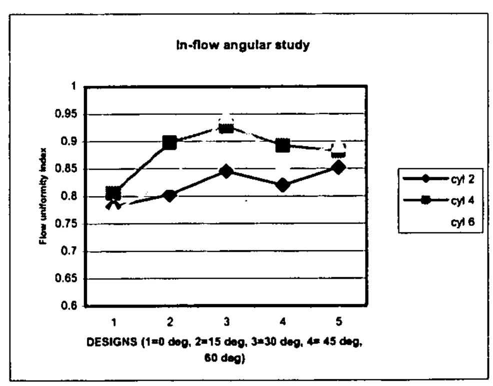

Figure 6. Graph showing gamma values at different flow deviation angles for cylinders 2, 4 and 6.

initially increase till the flow deviation angle is 30 degrees and they drop at 45 degree and again increase slightly at 60 degree. Hence it is concluded that 30 degree gives the highest flow uniformity index for the range of flow deviation angles considered.

Figure 7 shows velocity path lines for exhaust from cylinder 4 at zero degree flow deviation angle. Figure 8 shows the same at 30-degree flow deviation angle. It can be seen from Figure 7 that the at zero degree flow deviation angle, flow is mostly radial near the monolith entrance region causing more non-uniformity of flow. And it can be seen from Figure 8 that the flow is relatively smooth near the monolith entrance region at 30-degree deviation angle compared to flow at zero-degree deviation angle.

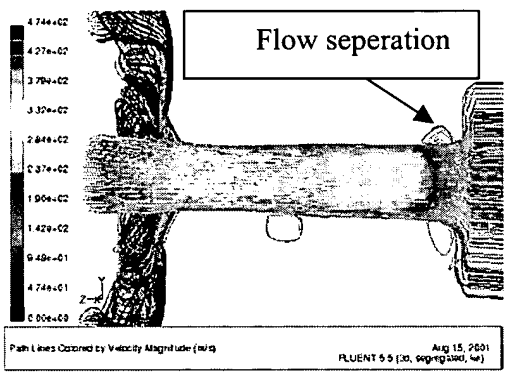

Figure 7. Velocity path lines due to exhaust from cylinder 4 at zero-degree flow deviation angle.

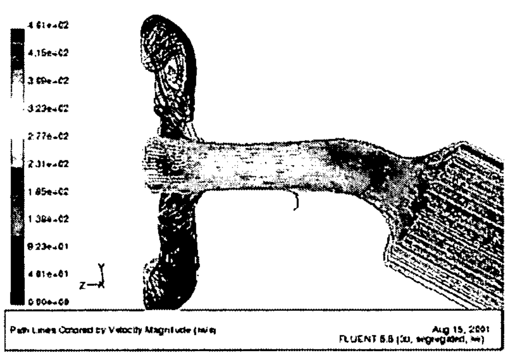

Figure 8. Velocity path lines due to exhaust from cylinder 4 at 30-degree flow deviation angle.

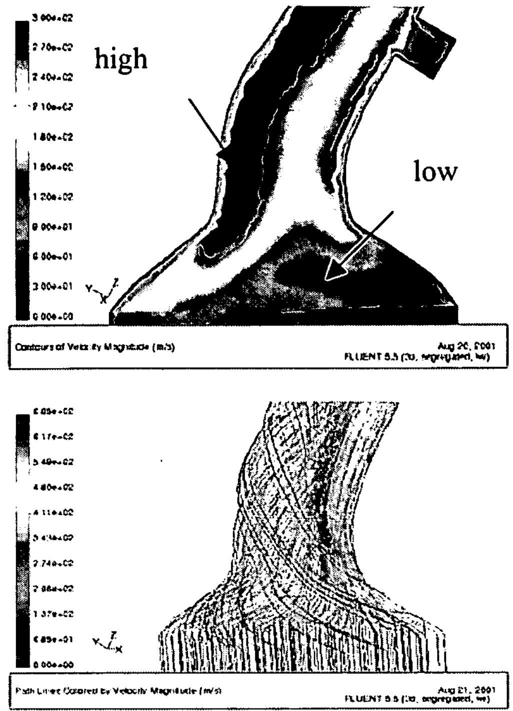

Figure 9. Velocity contours and path lines due to exhaust from cylinder 2 at 30-degree flow deviation angle.

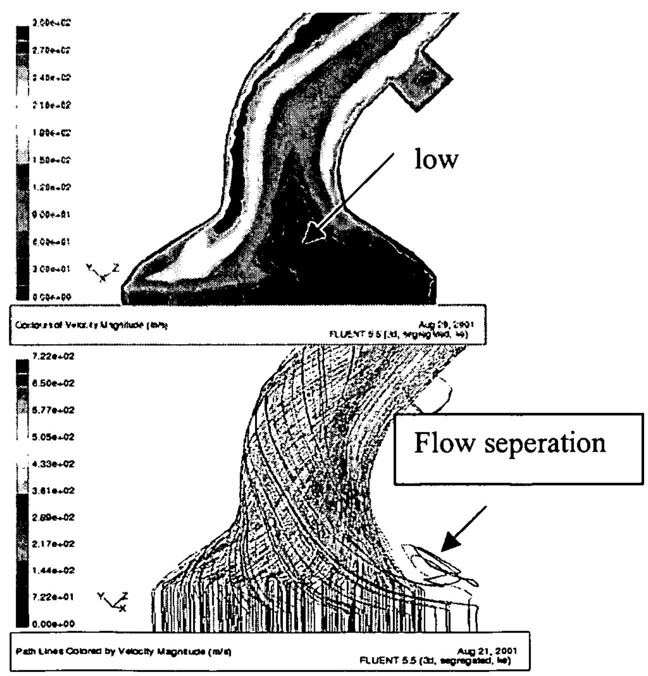

Figure 10. Velocity contours and path lines due to exhaust from cylinder 2 at 45-degree flow deviation angle.

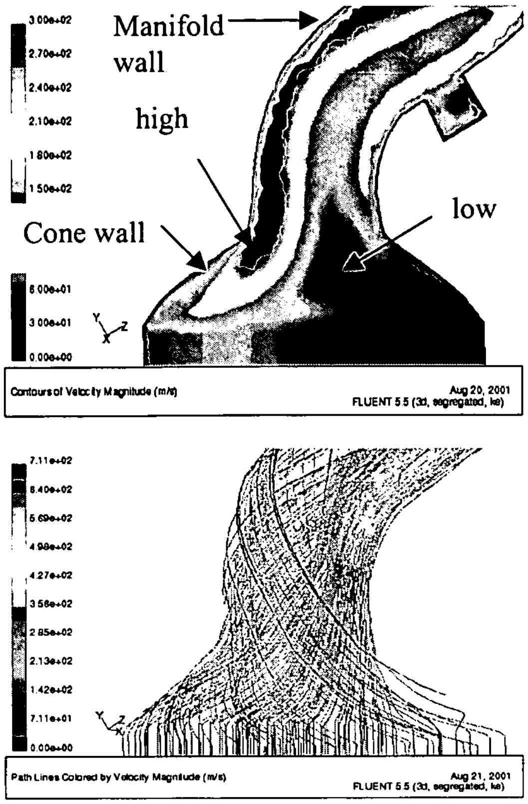

Figure 11. Velocity contours and path lines due to exhaust from cylinder 2 at 60-degree flow deviation angle.

It can be seen from Figure 6, gamma increases till flow deviation angle of 30 degree and drops at 45 degree and then again increases at 60 degree. This can be explained from Figures 9, 10 and 11. These Figures show velocity contours for exhaust flow from cylinder 2 at 30, 45 and 60 degrees. Comparing Figures 9 and 10, it can be seen that, almost constant high velocity region becomes thin in the 45-degree case. This cause higher non-uniformity (flow separation, see Figure 10) in the flow in 45-degree angle case and hence decrease in gamma value. Comparing Figures 10 and 11, it can be seen that almost constant high velocity region increases again in the 60-degree case. Hence there is more flow uniformity in 60-degree case compared to 45-degree case. This results in higher gamma value in 60-degree case compared to 45-degree case. It can also be noted from Figure 11 that, the manifold wall is almost parallel to cone wall on the left side of the Figure.

Figure 9 shows the values of total pressure drop from inlet to outlet for cylinders 2, 4 and 6 for flow deviation angles from 0 degree to 60 degree. It can be seen from Figure 9 that although pressure drop varies for the flow deviation angles considered here, for the center head (cylinder 4) of the manifold the pressure drop is considerably lower compared to pressure drops corresponding to other heads (cylinders 2 and 6).

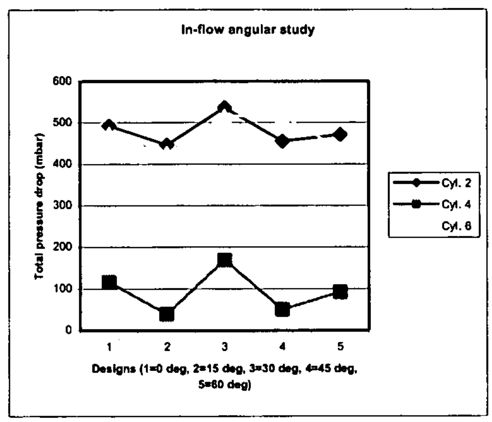

Figure 9. Total pressure drop versus flow deviation angle for cylinders 2, 4 and 6.

UNDER FLOOR CONVERTER:

The study of an isolated (under) floor converter with out the manifold is considered here to see how an under-floor converter, similar to close-coupled converter, behaves when the flow deviation angle is changed from 0 degree to 90 degree.

In the under-floor converter case, the same inlet & outlet cones, and monolith, as used in the close-coupled converter, are considered. The outlet tube is a straight tube. The other flow conditions are same as in the close-coupled case. The inlet tube shape is changed according to flow

deviation angles, keeping a constant inlet tube length, with the bend at the center of the tube length and the bend radius equals two times the diameter of the tube.

Figure 10. Shows the gamma value for flow deviation angles from zero degree to 90 degrees.

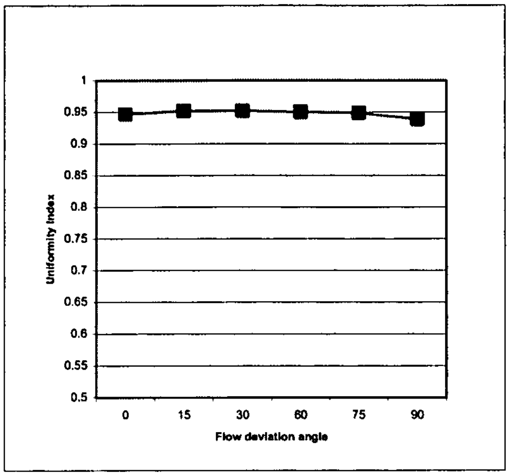

Figure 10. Flow uniformity index versus flow deviation angles for under floor converter case.

It can be seen from Figure 10 that the gamma values remain constant at 0.945 with in a range of 0.11 for all angles from 0 degree to 90 degrees. Figure 11, 12 and 13 show velocity contours for flow deviation angles of 30, 60 and 90 degrees. It can be seen from these Figures that the degree of uniformity/non-uniformity is almost same for all these cases. Hence in an isolated under-floor converter case it is possible to obtain almost constant flow uniformity index for any angle from 0 degree to 90 degrees.

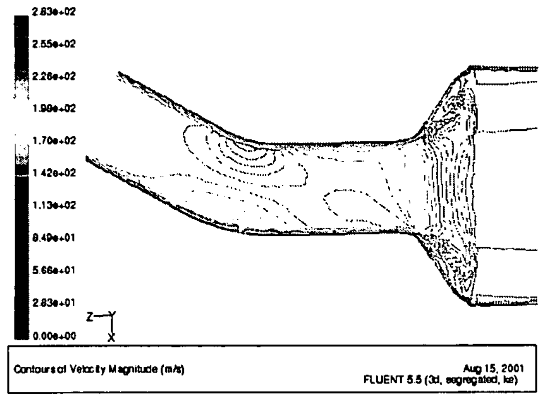

Figure 11. Velocity contours for 30 degree flow deviation angle in the under floor converter case.

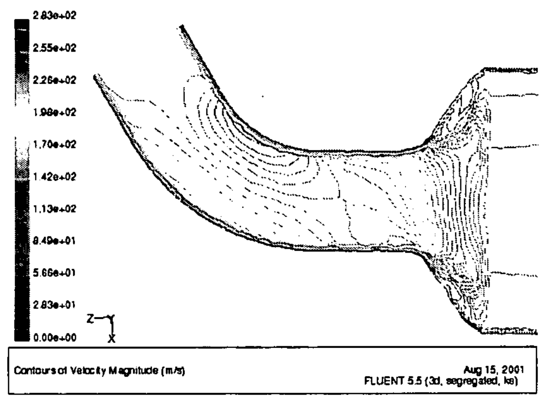

Figure 12. Velocity contours for 60 degree flow deviation angle in the under floor converter case.

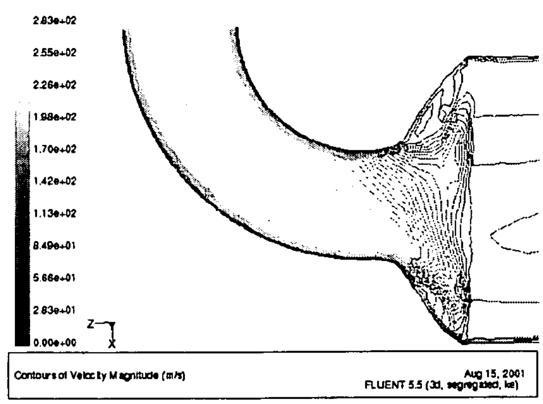

Figure 13. Velocity contours for 90 degree flow deviation angle in the under floor converter case.

STRUCTURAL BEHAVIOUR OF MANIFOLD UNDER EXHAUST LOADING:

The manifolds are subjected to extreme temperatures. The temperatures can go as high as 950 C and it can cool down from 950 C to room temperature, 20 C. Several such heating and cooling phases will create high stresses and strains in the manifold. Depending on the material, design and temperature, maximum stresses/strains can be caused either during heating stage or during cool down phase. Due to such severe loads, the structural analysis of exhaust manifold need to consider both material and geometric non-linearity. This study involves the behavior of steel manifolds under few heating and cooling cycles with out considering the effects of creep and fatigue. Further a comparative analysis between the behavior of cast steel and hydro formed/fabricated manifold under such loadings is carried out.

MECHANICAL RESPONSE OF A CAST STEEL MANIFOLD:

The manifold considered is shown in Figure 14. It is made of a particular type of cast austenitic stainless steel. The thickness of manifold is 6.0 mm and thickness of flange is 10 mm. The boundary conditions consist of constraining near the flange bolt holes and temperature distribution on the manifold surface is obtained from CFD analysis. The CFD analysis was performed using peak exhaust gas conditions. The manifold is subjected to heating from room temperature to temperature distribution corresponding to peak exhaust gas conditions. The manifold obviously expands during this stage. The manifold is then cooled back to room temperature. The manifold is subjected to few such heating and cooling cycles and the stress/strain response is studied.

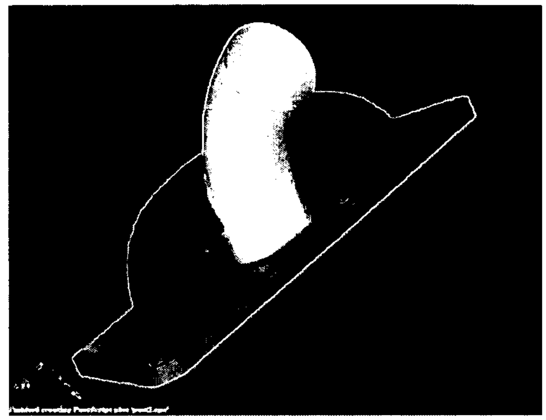

Figure 14. Manifold used in thermal stress/strain analysis.

The mechanical response is studied using strain and stress results during heating and cooling cycles. The plastic strain response at a critical point (on manifold) for the cast steel manifold is shown in Figure 15. And the corresponding stress response is shown in Figure 16. It is clear from the strain response that, the peak plastic strains during both heating and cooling cycles increases with the number of cycles. The corresponding stress response as seen from Figure 16 indicates that extreme (maximum and minimum) principal stress remain almost constant. This indicates that creep is occurring at this point in the manifold at high temperatures.

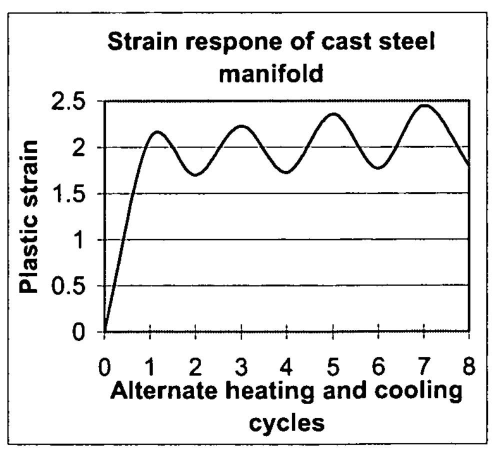

Figure 15. Strain response of cast steel manifold during alternate heating and cooling cycles.

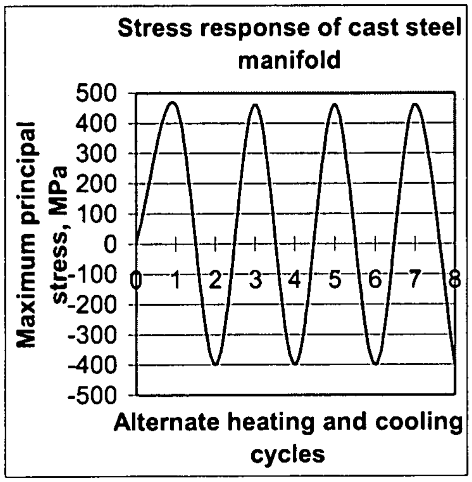

Figure 16. Stress response of cast steel manifold during alternate heating and cooling cycles.

MECHANICAL RESPONSE OF A HYDROFORMED STEEL MANIFOLD:

The hydroformed manifold is made almost similar in shape as cast manifold so that its flow performance is not changed. The type of steel selected has properties similar to those of the cast steel. The hydroformed manifold is made of two components. They are laser cut and joined together at the interface by welding. The manifold considered is shown in Figure 14. The thickness of the manifold is 2.0 mm and the flange thickness is 10.0 mm. The hydroformed steel manifold is subjected to alternate heating and cooling under conditions similar to the one used in the cast steel manifold. The strain and stress responses at a critical point on the manifold are shown in Figures 17 and 18 respectively.

In this case, for the point (element) under consideration, the plastic strains remain constant both in heating and cooling cycles even when the cycles are increased in number. The maximum and minimum principal stresses increase slightly initially and then stay at constant values.

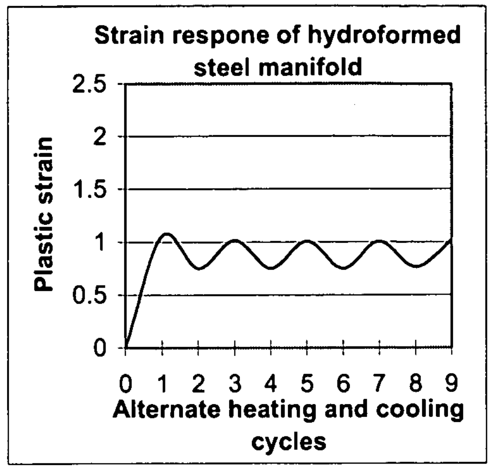

Figure 17. Strain response of hydroformed steel manifold during alternate heating and cooling cycles.

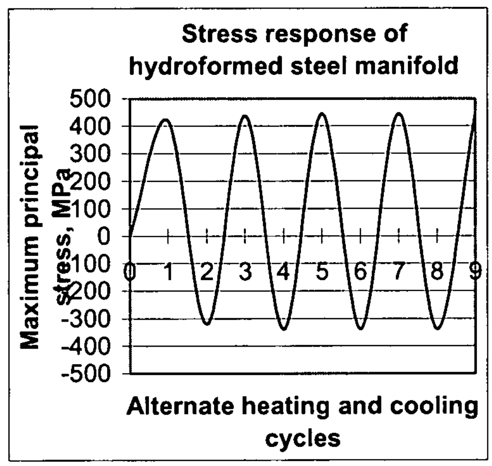

Figure 18. Stress response of hydroformed steel manifold during alternate heating and cooling cycles.

CAST VERSUS HYDROFORMED STEEL MANIFOLDS:

When comparing responses in both the cases, most critical points on the skin of the manifolds are considered. Table 3 shows details of stresses and strains for both cast austenitic stainless manifold and hydrofomed stainless steel under alternate heating and cooling cycles. It is clear from table 3 that, strains produced in cast steel manifold are more than twice those obtained for hydrofomed stainless steel manifold.

Hence structural performace of hydroformed manifold is superior to cast stainless steel manifold during heating under exhaust gas conditions and cooling cycles.

Considering vibration loads, the vibration response of exhaust system with the thin hydroformed/stamped manifold can be tailored to behave such that it produces an acceptable NVH behavior, by manipulating the hangers, decouplers, etc.

In addition, the tubular/shell/hydroformed steel manifolds also have some advantages considering light-off, weight and cost compared to cast steel manifolds.

CONCLUSION:

1. CFD optimization analysis of exhaust systems having close-coupled converter with same front and back cones with varying in-flow deviation angles and different exit tube profiles are carried out
2. It is shown that exit tube shape and direction of outflow can affect the flow distribution in front of the catalyst monolith.
3. For the system under consideration, It is shown that flow uniformity index initially increase with increase in flow-deviation angle and then decrease and again increase with in-flow deviation angle.
4. The second hump or increase in flow uniformity index occurs when the tube profile (at 60 degrees) is parallel to the skin of the front cone.
5. Under certain conditions, it is shown that almost constant and maximum flow uniformity index can be obtained for isolated converters (under flow converters) with the same front and back cones for all flow deviation angles of 0 degree to 90 degrees.
6. Thermo-Mechanical response of manifolds subjected to several alternate heating and cooling cycles is calculated.
7. It is shown that hydroformed/fabricated stainless manifolds produce considerably less strains/stresses compared to similar manifolds made of cast stainless steel manifolds.

ACKNOWLEDGEMENTS:

The first author would like to thank Drs. Joachim Braun, Joachim Hildebrand and Ralf Riekers of J. Eberspaecher GmbH & Co. for sharing the material properties data and their expertise.

REFERENCES:

1. H. Weltens, H. Bressler, F. Terres, H. Newmaier, & D. Rammoser, Optimization of catalytic converter gas flow distribution by CFD prediction, 1993 SAE Internal Congress and Exposition, SAE paper no. 930780.
2. S. Jeong and T. Kim, CFD investigation of the 3-Dimensional unsteady flow in the catalytic converter, 1997 SAE Internal Congress and Exposition, SAE paper no. 971025.
3. H. Kim, S. Park, C. Myung, K. Cho and K. Yoon, A study of flow characteristics inside the two types of exhaust manifold and CCC systems, 1999 SAE Internal Congress and Exposition, SAE paper no. 1999-01-0457.
4. A. Martin, N. Will A. Bordet and P. Cornet, C. Gondoin, and X. Mouton, Effect of flow distribution on emissions performance of catalytic converters, 1998 SAE Internal Congress and Exposition, SAE paper no. 980936.
5. D. Anderson, D. Bisaro, D. Haan and M. Olree, A thermoviscoplastic FE model for the strain prediction in high temperature, thermal cycling applications for silicon molybdenum nodular cast iron, 1998 SAE Internal

Congress and Exposition, SAE paper no. 980697.

6. Y. Watanabe, K. shiratani, S. Iwanaga and K. Nishino, Thermal fatigue life prediction for stainless steel exhaust manifold, 1998 SAE Internal Congress and Exposition, SAE paper no. 980841.
7. G. Lederer, E. Charkaluk, L. Verger, A. Constantinescu, Numerical lifetime assessment of engine parts submitted to thermomechanical fatigue, application to exhaust manifold design, 2000 SAE Internal Congress and Exposition, SAE paper no. 2000-01-0789.

CONTACT:

lakshmikantha.meda@eberspaecher.com

Manifold type	Strain/stress	Heating	Cooling
	Plastic strain (avg. of peaks)	2.3	1.75
Cast stainless Steel	Max. principal stress (MPa)	462	-400
	Von-Mises	400	400
	Plastic strain (avg. of peaks)	1	0.75
Hydroformed stainless steel	Max. principal stress (MPa)	445	-339
	Von-Mises stress (MPa)	386	386

Table 3. The structural response data of two types of manifolds at critical points on the manifold wall.